Optical band gaps and composition dependence of hafnium–aluminate thin films grown by atomic layer chemical vapor deposition

N. V. Nguyen, S. Sayan, I. Levin, J. R. Ehrstein, I. J. R. Baumvol, C. Driemeier, C. Krug, L. Wielunski, P. Y. Hung, and Alain Diebold

Citation: Journal of Vacuum Science & Technology A **23**, 1706 (2005); doi: 10.1116/1.2091096
View online: https://doi.org/10.1116/1.2091096
View Table of Contents: https://avs.scitation.org/toc/jva/23/6
Published by the American Vacuum Society

ARTICLES YOU MAY BE INTERESTED IN

Energy gap and band alignment for $(HfO_2)_x(Al_2O_3)_{1-x}$ on (100) Si
Applied Physics Letters **81**, 376 (2002); https://doi.org/10.1063/1.1492024

Crystal structure and band gap determination of HfO_2 thin films
Journal of Applied Physics **101**, 054101 (2007); https://doi.org/10.1063/1.2697551

Spectroscopic ellipsometry characterization of high-k dielectric HfO_2 thin films and the high-temperature annealing effects on their optical properties
Applied Physics Letters **80**, 1249 (2002); https://doi.org/10.1063/1.1448384

High-κ gate dielectrics: Current status and materials properties considerations
Journal of Applied Physics **89**, 5243 (2001); https://doi.org/10.1063/1.1361065

Parameterization of the optical functions of amorphous materials in the interband region
Applied Physics Letters **69**, 371 (1996); https://doi.org/10.1063/1.118064

Sub-bandgap defect states in polycrystalline hafnium oxide and their suppression by admixture of silicon
Applied Physics Letters **87**, 192903 (2005); https://doi.org/10.1063/1.2126136

Optical band gaps and composition dependence of hafnium–aluminate thin films grown by atomic layer chemical vapor deposition

N. V. Nguyen[a)]
Semiconductor Electronics Division, National Institute of Standards and Technology, Gaithersburg, Maryland 20899

S. Sayan
Department of Chemistry, Rutgers University, Piscataway, New Jersey 08854

I. Levin
Ceramics Division, National Institute of Standards and Technology, Gaithersburg, Maryland 20899

J. R. Ehrstein
Semiconductor Electronics Division, National Institute of Standards and Technology, Gaithersburg, Maryland 20899

I. J. R. Baumvol and C. Driemeier
Instituto de Fisica, UFRGS, 91509-900 Porto Alegre, RS, Brazil

C. Krug
Department of Physics, North Carolina State University, Raleigh, North Carolina 27695

L. Wielunski
Department of Physics and Astronomy, Rutgers University, Piscataway, New Jersey 08854

P. Y. Hung and Alain Diebold
International Sematech, Austin, Texas 78741

(Received 30 September 2004; accepted 29 August 2005; published 25 October 2005)

We report the optical properties of unannealed hafnium–aluminate (HfAlO) films grown by atomic layer chemical vapor deposition (ALCVD) and correlate them with the aluminum contents in the films. Vacuum ultraviolet spectroscopic ellipsometry (VUV-SE), high-resolution transmission electron microscopy (HRTEM), channeling Rutherford backscattering spectrometry (RBS), and resonant nuclear reaction analysis (NRA) were employed to characterize these films. In the analyses of ellipsometry data, a double Tauc–Lorentz dispersion produces a best fit to the experimental VUV-SE data. As a result, the determined complex pseudodielectric $\langle \varepsilon \rangle$ functions of the films clearly exhibit a dependency on the aluminum densities measured by RBS and NRA. We show that the optical fundamental band gap E_g shifts from 5.56 ± 0.05 eV for HfO_2 to 5.92 ± 0.05 eV for HfAlO. The latter was grown by using an equal number of pulses of $H_2O/HfCl_4$ and H_2O/TMA (trimethylaluminum) precursors in each deposition cycle for HfO_2 and Al_2O_3, respectively. The shift of E_g to higher photon energies with increasing aluminum content indicates that intermixing of HfO_2 and Al_2O_3 occurred during the ALCVD growth process. We found that E_g varies linearly with the mole fraction x of Al_2O_3 in the alloy $(HfO_2)_x(Al_2O_3)_{1-x}$, but has a parabolic dependency with the aluminum density. We also observed a consistent decrease in the magnitudes of the real $\langle \varepsilon_1 \rangle$ and imaginary $\langle \varepsilon_2 \rangle$ part of $\langle \varepsilon \rangle$ of HfAlO films with respect to those of HfO_2 as the Al density increased. The absence of the ≈ 5.7 eV peak in the $\langle \varepsilon \rangle$ spectrum, which was previously reported for polycrystalline HfO_2 films, indicates that these films are amorphous as confirmed by their HRTEM images. © *2005 American Vacuum Society.* [DOI: 10.1116/1.2091096]

I. INTRODUCTION

High-k dielectric thin films have been the subject of a strong focus in the past years within the integrated circuit (IC) industry and academic research communities as a potential replacement for the traditional SiO_2 gate dielectric in complementary metal–oxide–semiconductor devices.[1] According to the International Technology Roadmap for Semiconductors, SiO_2 gate thicknesses of less than 2 nm will be required in sub-0.1 μm MOS devices.[2] In this range of thickness, the use of the SiO_2 and SiO_xN_y layers as dielectric gates will not be acceptable for many applications due to the high tunneling currents. By exploiting the higher permittivity of high-k dielectrics, one can grow a physically much thicker gate dielectric layer while still having thinner SiO_2 equivalent oxide thickness (EOT)[3] and, thereby, significantly reduce the tunneling leakage currents. Various high-k materials have been examined including $Ta_2O_5, TiO_2, Al_2O_3, ZrO_2$, HfO_2, Zr–silicates, Zr–aluminates, and Hf–aluminates.[4] Among these possible candidates, HfO_2 has been considered as a likely replacement for SiO_2 due to its high permittivity

[a)]Electronic mail: nhan.nguyen@nist.gov

TABLE I. Summary of the experimental results obtained from the VUV-SE, RBS, and NRA measurements. Targeted film composition is denoted by $\boldsymbol{n}[\boldsymbol{p}(\mathrm{HO}):\boldsymbol{q}(\mathrm{AO})]$ where $\boldsymbol{p}$ is number of H_2O/TMA cycles followed by $\boldsymbol{q}$ cycles of $H_2O/HfCl_4$; and this sequence is repeated n times. The targeted film composition $\boldsymbol{q}:\boldsymbol{p}$ ratio controls the composition x of the $(HfO_2)_x(Al_2O_3)_{1-x}$ alloy (see text of Fig. 6). The film thicknesses and optical band gaps (E_g) are obtained from modeling the spectroscopy ellipsometry data. The aluminum concentrations (Q_{Al}) in units of 10^{15} atoms/cm^2 are determined by NRA whereas those of hafnium (Q_{Hf}) and oxygen (Q_O) determined by RBS. The estimated precision is ±10% for Al concentrations unless otherwise stated. The estimated concentration precisions are ±3%, ±10%, and ±30% for Hf, O, and Cl, respectively.

Samples	Composition $\boldsymbol{n}[\boldsymbol{p}(\mathrm{HO}):\boldsymbol{q}(\mathrm{AO})]$	Thickness (Å)	$E_g \pm 0.05$(eV)	Q_{Hf}	Q_{Al}	Q_O	Q_{Cl}
S2	30[1(HO):1(AO)]	51.5	5.97	5.3	10.2	25.5	0.2
S5	40[1(HO):1(AO)]	64.5	5.88	6.5	13.7	29.6	0.3
S7	50[1(HO):1(AO)]	77.1	5.91	9.0	19.5	43.5	0.4
S9	15[5(HO):1(AO)]	60.7	5.68	12.9	4.3	38.0	0.5
S12	20[5(HO):1(AO)]	78.9	5.72	15.9	5.8	43.1	0.5
S14	25[5(HO):1(AO)]	93.2	5.76	18.9	7.7	46.7	0.5
S16	74[5(HO):0(AO)]	48.1	5.58	11.1	-	25.0	0.3
S19	92[5(HO):0(AO)]	56.3	5.54	13.7	-	28.8	0.3
S21	[37(HO):5(AO):37(HO)][a]	52.2	5.62	10.8	2.0±0.4	29.1	0.3
S24	[46(HO):5(AO):46(HO)][a]	61.1	5.58	13.4	2.2±0.4	31.9	0.3

[a]The growth sequence consisted of 37 or 46 H_2O/TMA cycles followed by 5 cycles of $H_2O/HfCl_4$ and finished with 37 or 46 H_2O/TMA cycles.

and thermodynamic stability with silicon.[5] However, in the subsequent fabrication steps, the stability of HfO_2 against crystallization improves significantly upon alloying with Al_2O_3 to form Hf–aluminates.[6–8]

This article shows that vacuum ultraviolet spectroscopic ellipsometry (VUV-SE) is able to correlate the optical properties and optical bandgap (E_g) of Hf–aluminate films with their aluminum composition. Due to the relatively large band gaps (3.5–7 eV) of most high-k materials of technological importance, VUV-SE with a spectral range extended to $\approx$9.0 eV was found to be the most suitable technique to ascertain the optical properties near and above the fundamental band gap.[9–13] In this spectral range, E_g can be readily determined. We show that the E_g value deduced experimentally varied with the amount of the Al_2O_3 used to grow Hf–aluminate films. Complementary experiments including high-resolution electron transmission microscopy (HRTEM), channeling Rutherford backscattering spectrometry (RBS), and resonant nuclear reaction analysis (NRA) were also performed on the same set of films to evaluate the interface layer, film thickness, and atomic concentrations of hafnium, oxygen, and aluminum. We observe that the determined complex pseudodielectric functions ($\langle\varepsilon\rangle=\langle\varepsilon_1\rangle+i\langle\varepsilon_2\rangle$) of the HfO_2 and HfAlO films exhibit a shift of the fundamental band gap E_g from 5.56 eV for HfO_2 to 5.92 eV for HfAlO where the latter was grown with an equal (1:1) ratio of HfO_2 and Al_2O_3. We also observe a consistent decrease in the magnitudes of $\langle\varepsilon_1\rangle$ and $\langle\varepsilon_2\rangle$ of HfAlO films with respect to that of HfO_2 as the Al density increased. Further, the broad feature above the band gap in the $\langle\varepsilon\rangle$ spectrum indicates the amorphous structure of the as-grown films. HRTEM images confirmed the amorphous nature of the films. With respect to the oxygen density, RBS and NRA results indicate an apparently slight oxygen deficiency.

II. EXPERIMENT AND DATA ANALYSIS

A series of ten wafers of HfO_2 and Hf–aluminate films of different thicknesses and various content of Al was employed in this study. These films were deposited by atomic layer chemical vapor deposition (ALCVD). In ALCVD, precursors are introduced alternately to the silicon substrate with inert gas purged between each introduction. The two precursors pulsed in each deposition cycle consist of $H_2O/HfCl_4$ (hafnium tetrachloride) for HfO_2 deposition and H_2O/TMA (trimethylaluminum) for Al_2O_3 deposition. The growth sequence, denoted by $n^*(p\mathrm{AO}:q\mathrm{HO})$, is listed in Table I, where p is number of H_2O/TMA cycles followed by q cycles of H_2O/HfC_{14}, and then, these two sets of cycles were repeated n times. Therefore, the ratio of p and q controls the composition and the total number of cycles n determines the film thickness. The reactive precursor absorbs chemically on the wafer surface and undergoes a self-limiting reaction, and consequently a monolayer film growth can be achieved.[14] As a result, a uniform and conformal growth is attainable, and the film thickness can be easily controlled by setting the total number of growth cycles. In our experiment, after the standard SC1/SC2 wet chemical cleaning of silicon substrates, a thin layer of rapid thermal SiO_2($\approx$1.2 nm) was grown to be used as active surface sites for the subsequent film growth. Such a thin SiO_2 layer has been shown to be necessary to facilitate a uniform film growth, to ensure a linear growth rate, and also to achieve a well-controlled and well-behaved growth of films of amorphous structure at low temperatures.[15] Various targeted film compositions were deposited as shown in Table I.

All spectroscopic ellipsometry measurements were performed on a vacuum ultraviolet spectroscopic ellipsometer (SE). The measured spectral range was scanned from 1.5 to

9.0 eV, in steps of 0.01 eV and the angle of incidence was set at 75°. To determine the thickness and the pseudodielectric functions of each film, we utilized a model consisting of the crystalline silicon (*c*-Si) substrate, the interfacial layer of SiO_2, and the HfO_2 or Hf–aluminate film. The incorporation of the SiO_2 interfacial layer of 11 Å in the model was justified by the HRTEM images (Fig. 1) measured for samples S5 and S9 and the same SiO_2 thickness is assumed for all samples. The uncertainty of the SiO_2 thickness is about 1.5Å which was found to have negligible effects on the SE results, specifically on the determination of the optical band gaps of the films. The dielectric function of the Si substrate extended to 8.3 eV, and the refractive indices of SiO_2 were obtained from the literature.[16] To fit the experimental ellipsometric data, Δ and Ψ, the dielectric function of the films is assumed to follow a dielectric dispersive relation. The most used dispersion equation for amorphous materials is the Tauc–Lorentz (TL) developed by Jellison and Modine.[17] In this dispersion, the real part (ε_1) of the complex dielectric function (ε) is obtained by multiplying the imaginary part (ε_2) expression of the Lorentz oscillator and the Tauc joint density of states. ε_1 was then analytically deduced from ε_2 by use of the classical self-consistency Kramer–Kronig integration:

$$\varepsilon_2(E) = \begin{cases} \dfrac{AE_0C(E-E_g)^2}{(E^2-E_0^2)^2+C^2E^2}\dfrac{1}{E} & (E > E_g) \\ 0 \quad (E < E_g), \end{cases}$$

$$\varepsilon_1(E) = \varepsilon_\infty + \frac{2}{\pi}P\int_0^\infty \frac{\xi\varepsilon_2(\xi)}{\xi^2-E^2}d\xi,$$

where A, E_g, E_0, and C are positive constant fitting parameters in units of energy, and, ε_∞ is a dimensionless fitting constant. All the TL fitting parameters and film thicknesses were deduced from the biased least squares.

The phase contrast imaging and electron energy loss spectroscopy (EELS) were conducted in a JEOL-3010-UHR (300 kV) HRTEM equipped with a Gatan imaging filter (GIF) and a slow-scan CCD camera. The EELS experiments were conducted by rotating the HRTEM image so that the interfaces were set parallel to the energy-dispersion direction of the GIF. The analyzed area was selected by the GIF entrance aperture. The EELS spectra containing low-loss regions and characteristic Hf $N_{4,5}$, SiAl $L_{2,3}$, Si $L_{2,3}$, and O K edges were recorded with an energy dispersion of 0.1 eV/ch. Under the chosen experimental conditions, spatial resolutions of about 1 nm were obtained. HRTEM images of samples S5 and S9 are shown in Fig. 1. According to the EELS analysis, the upper dark layers in both images correspond to amorphous Hf–aluminate whereas the interfacial layer about 1.1 nm thick was identified with silicon oxide.

RBS was performed in channeling configuration to quantify Hf, O, and Cl. The $\langle 001 \rangle$ axis of Si(100) substrates was aligned to the direction of incidence of a He^+ primary beam at 1 MeV. Scattered particles were detected at 110° with respect to the direction of ion beam incidence. Elemental

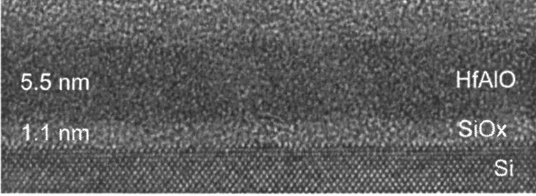

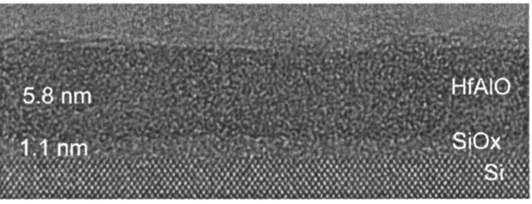

FIG. 1. HRTEM images for samples S5 and S9 used to determine the interface SiO_2 layer of thickness 11 Å in the SE data analysis.

amounts (areal densities) Q_i were calculated from the area of the RBS signals, referenced to a Harwell series II Si(Bi) standard and corrected for the change in cross section. The estimated precision in these measurements is ±3% for Hf, ±10% for O, and ±30% for Cl. No carbon was detected, indicating an areal density below 10^{16} cm^{-2}.

NRA was performed to quantify and profile aluminum. Quantification was accomplished by using the narrow (FWHM <100 eV) resonance at 992.0 keV in the cross-section curve of the $^{27}Al(p,\gamma)^{28}Si$ reaction. Proton incidence was normal to the sample surface, and gamma rays were detected along the direction of proton incidence (behind the samples). Al amounts (areal densities) Q_{Al} were calculated from the area under excitation curves (not shown) after background subtraction and normalization for the number of incident protons, by using a standard Al_2O_3 film on Si as reference. The estimated precision is ±10%.

Aluminum profiling was accomplished by using the narrow (FWHM <40 eV) resonance at 404.9 keV in the cross-section curve of the above-mentioned reaction. Proton incidence was at 60° with respect to the normal to the sample surface, and gamma rays were again detected along the direction of proton incidence. Profiles were obtained from simulations of the experimental excitation curves by using the FLATUS program. The depth scale in the profiles was estimated by using (i) hafnium and aluminum areal densities, (ii) the calculated stopping power for protons in $(HfO_2)_x(Al_2O_3)_{1-x}$ (in units of mass per area), and (iii) weighted averages of Al_2O_3 and HfO_2 densities, respectively, 4.0 and 9.7 g/cm^3. Table I summarizes the elemental characterization data.

III. RESULTS AND DISCUSSION

In fitting the VUV-SE data with a single TL oscillator, we found that there was a large discrepancy between the mod-

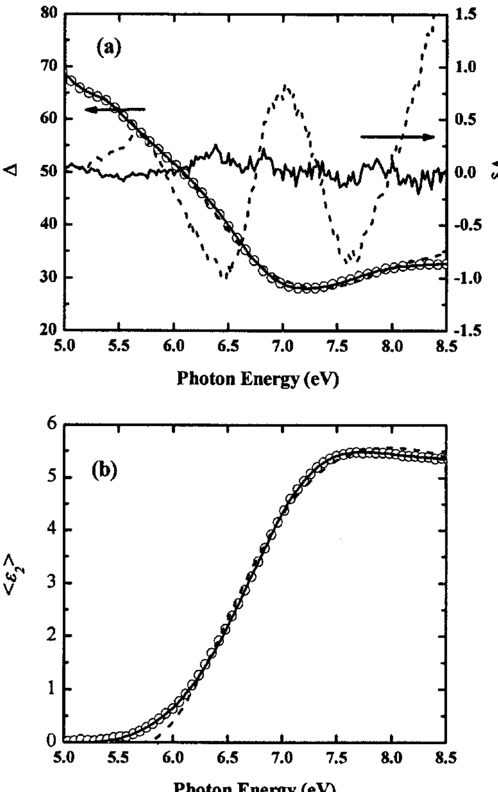

FIG. 2. (a) Comparisons between the experimental (open circles) and modeled (dashed line for the single TL and solid line for the double TLs) data (Δ) for sample S16. Fitting error $\delta\Delta$ depicts an excellent fit for the double TL model (solid line) compared with that of the single TL model (dashed line). (b) The corresponding inverted imaginary (open circles) part $\langle\varepsilon_2\rangle$ of the pseudodielectric function $\langle\varepsilon\rangle$ is compared with the single (dashed line) and double (solid line) TL dispersions. For reference, the fitting parameters obtained from (i) the single TL model: $\varepsilon_\infty=1.527, A=596.36$ eV, $E_g=5.77$ eV, $E_0=6.13$, and $C=3.07$ eV, and (ii) the double TL model: $\varepsilon_\infty=1.234, A=154.21$ eV, $E_g=5.30$ eV, $E_0=7.04$ eV, and $C=2.23$ eV (the first TL) and $A=225.53$ eV, $E_g=6.85$ eV, $E_0=8.44$, and $C=4.63$ eV (the second TL).

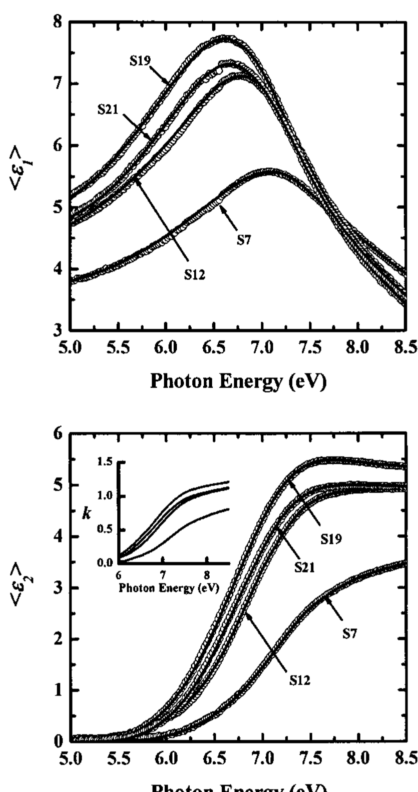

FIG. 3. Inverted dielectric functions (open circles), $\langle\varepsilon\rangle=\langle\varepsilon_1\rangle+i\langle\varepsilon_2\rangle$ and the fitting double Tauc–Lorentz oscillator dispersion (solid curves) obtained for samples S7, S12, S19, and S21. The inset of the bottom graph depicts the distinction coefficient k determined from $\langle\varepsilon_1\rangle$ and $\langle\varepsilon_2\rangle$.

eled and experimental data as displayed by the dashed curve in Fig. 2(a) for sample S16. Similar observations were made for all other samples (not shown). However, a sum of two TL oscillators improves the fit significantly, especially in the spectral range above 5.5 eV as depicted by the almost zero fitting error $\delta\Delta$ (solid curve in Fig. 2). With the double TL model, the data fitting of all samples results in the film thicknesses listed in Table I. To verify that the double TL dispersion is in fact a correct one for the films, we employed a data inversion to obtain the complex pseudo dielectric functions $\langle\varepsilon\rangle$ directly. In this inversion technique, $\langle\varepsilon_1\rangle$ and $\langle\varepsilon_2\rangle$ of the films were calculated from the measured Ψ and Δ, oint by point at each photon energy by using the film thickness obtained from the fit with the TL dispersion.[9] Figure 2(b) shows $\langle\varepsilon_2\rangle$ obtained by this inversion process (open circles) and from fitting the single (dashed curve) and double (solid curve) TL dispersions. The double TL dispersion is in excellent agreement with the calculated $\langle\varepsilon_2\rangle$, especially near the band gap, thus justifying the double TL dispersion model. Figure 3 depicts the representative (open circles) inversion $\langle\varepsilon\rangle$ spectrum compared with the modeled (solid curves) double TL dispersion obtained for samples S7 [1(HO): 1(AO)], S12 [51(HO): 1(AO)], S19 [1(HO): 0(AO)], and S21 [37(HO)/5(AO)/37(HO)]. The use of the double TL can be further justified by considering the energy band structure associated with transition metal/rare earth oxide modeled by Lukovsky *et al.*[18,19] To be specific, it was argued that the optical fundamental band gap or the lowest energy optical transition observed in the optical spectrum results from the transition between the highest occupied valence band of non bonding oxygen atom $2p-\pi$ states and the lowest Hafnium d-state conduction band. From the Tauc plot for samples S16 and S19, we obtained the band gap E_g for HfO_2 films, which are averaged to a value of 5.56 eV. This transition corresponds to the first TL oscillator. The second TL oscillator represents the second interband transition which is assumed to be associated with the (ionic band gap) transition between the highest occupied valence band of non bonding oxygen $2p-\pi$ state and the Hf s conduction band state.

One parameter of great interest is the optical band gap that we derive from the inverted dielectric functions. E_g is sensitive to the composition and electronic structure of HfO_2 and Hf–aluminate films as discussed in the following sections. Even though E_g's were obtained from fitting the data to the TL model, they are not accurate due to the correlation between the fitting parameters, especially in the case of the double TL model. In fact, all E_g's obtained from the single

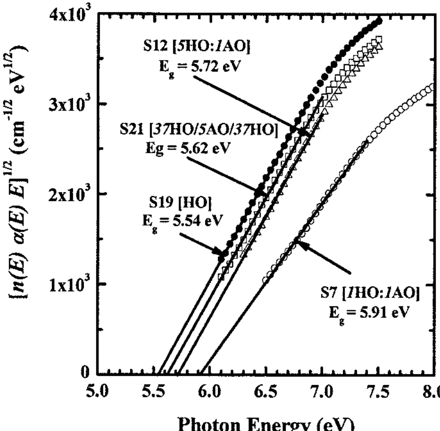

FIG. 4. Tauc plots for determining the optical band gap E_g which is the intercept of the linear fitting curve extrapolated to the zero absorption for samples S7, S12, S19, and S21. The uncertainty on E_g is ±0.05 eV.

TL model are about 0.3 eV below the real absorption edges (accurately determined in the following) whereas they vary widely in the double TL model. Generally, the band gap for an amorphous material is determined from the energy dependence of its absorption coefficient, $\alpha=4\pi k/\lambda$, near its absorption edge,[20] where λ is the photon wavelength and k is the extinction coefficient which can be calculated from ε_1 and ε_2 by the complex relation $(n+ik)^2=(\varepsilon_1+i\varepsilon_2)^2$ with n being the index of refraction. The most commonly used method to acquire E_g is to use the Tauc plot.[21] Tauc and co-workers showed that near the absorption edge of some amorphous materials, the expression $[n(E)\alpha(E)E]^{1/2}$ varies linearly with $(E-E_g)$ where E is the photon energy. If a straight line is obtained near the band edge in a plot of $[n(E)\alpha(E)E]^{1/2}$ versus the photon energy E, then the extrapolation to zero absorption results in the value of E_g. Figure 4 presents representative Tauc plots for samples S7, S12, S19, and S21. The portion of the spectrum between 6 and 7 eV near the band edge clearly follows a linear relationship with the photon energy E and was fitted to a straight line to obtain the bandgap values for all samples listed in Table I. The uncertainty of the E_g was estimated to be approximately 0.05 eV for all samples. The uncertainty was deduced from the worst case as if there was no SiO_2 interfacial layer used in the model or if the interface layer was not SiO_2 but a hafnium silicate or an understoichiometric SiO_x.

A. Optical band gap E_g and dielectric function of HfO_2

There have been numerous reported values for E_g of HfO_2. Table II compiles a limited survey of reported E_g of HfO_2 grown by various techniques and determined mainly by optical measurements. From our data analyses, E_g averaged on two HfO_2 samples (S16 and S19) of two different thicknesses is 5.56 eV. Boher *et al.*[13] employed both Grazing x-ray reflectance (GXR) and VUV-SE films and showed E_g to be approximately 5.5 eV from their HfO_2 $\langle\varepsilon\rangle$ spectrum. In a much earlier study by Balog *et al.*,[22] the E_g value of 5.65 eV of HfO_2 film, fabricated by CVD, was obtained by the use of the same Tauc-plot method on absorbance data. Our own most recent studies on a set of jet-vapor-deposited HfO_2 and Hf–aluminate films resulted in, however, a relatively lower E_g value of 5.08 eV for the HfO_2 film.[9] Lim *et al.*[23] performed a transmission measurement on an Y_2O_3-stabilized single crystalline HfO_2 and reported a higher E_g value of 5.8 eV. All of the just listed E_g's were determined with the measured spectral range above the band gap. In another study performed on a large set of MOCVD HfO_2 films by Modreanu *et al.*[24] using only the data measured in a limited range of photon energy up to 4.5 eV, much below the band gap, they managed to deduce E_g by using an empirical formula that relates the strength of the interband optical transitions. However, their E_g were shown to vary in a wide range from 5.66 to 5.95 eV, possibly due to their samples experiencing various postgrowth annealing and the lack of experimental data above the band gap. For a comparison with a more elaborate physical technique such as the x-ray photoelectron spectroscopy (XPS) performed by Yu *et al.*[25] on ALD $(HfO_2)_x(Al_2O_3)_{1-x}$, a lower E_g value of 5.25 eV for HfO_2 was calculated from the onset of the O 1*s* band energy loss XPS spectra. In a recent internal electron photoemission study of ALD HfO_2,[26] E_g was determined from the photoconductivity spectra and found to be 5.6 eV in a good agreement with this report. Overall, E_g varies in a range from ≈5 to ≈6 eV dependent on the techniques used to grow the films, as well as the particular *optical* characterization tool and the corresponding model used to determine E_g.

Another quantity that relates to the film structural quality is the relative magnitude of $\langle\varepsilon_1\rangle$ and $\langle\varepsilon_2\rangle$. In the following we compare $\langle\varepsilon_1\rangle$ and $\langle\varepsilon_2\rangle$ obtained for our HfO_2 films with those published elsewhere. The Y_2O_3-stabilized HfO_2 single

TABLE II. Brief survey of the E_g reported in published literature.

Preparation method	$E_g(HfO_2)$(eV)	Optical techniques	References
ALCVD	5.56	VUV-SE (1.5–8.3 eV)	This article
ALCVD	≈5.5[a]	VUV-SE	Boher *et al.*[13]
CVD	5.65	Absorbance	Balog *et al.*[22]
HfO_2 single crystal	5.8	Transmission	Lim *et al.*[11]
Jet-vapor deposition	5.08	VUV-SE (1.5 – 8.3 eV)	Nguyen *et al.*[9]
MOCVD	5.66–5.95	SE (1.5 – 4.5 eV)	Modreanu *et al.*[24]

[a]This value was not reported but estimated from $\langle\varepsilon_2\rangle$ spectrum.

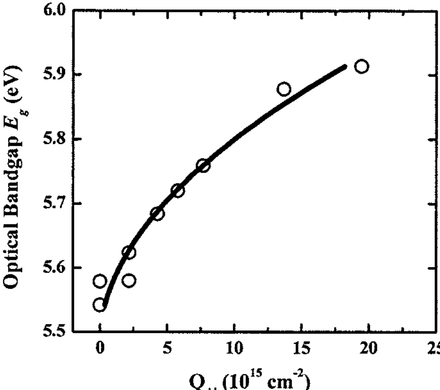

FIG. 5. Variation of E_g determined by VUV-SE varies with respect to the aluminum (areal) density in the film obtained from NRA measurements. The solid line is a linear fit where the band gap E_g of the endpoint of Al_2O_3 (not available in this study) was taken from our previous study (Ref. 9).

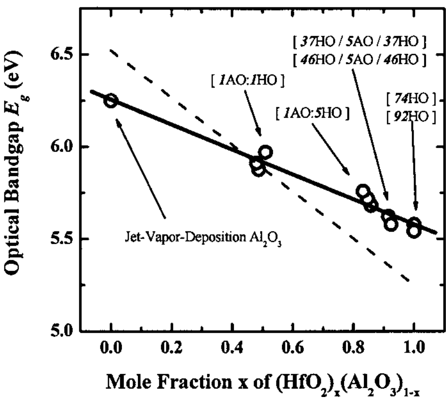

FIG. 6. Plot of E_g versus the mole fraction x of the $(HfO_2)_x(Al_2O_3)_{1-x}$ alloyed films. The solid line (E_g=6.26−0.68 x) is the linear least squares fitting of E_g. The dashed curve is the linear relation (E_g=6.52−1.27 x) reported by Yu *et al.*[25]

crystal of Lim *et al.*[23] showed higher values of $\langle\varepsilon_1\rangle$ and $\langle\varepsilon_2\rangle$. Their peak values in $\varepsilon_1(\approx 10.5)$ and $\varepsilon_2(\approx 8.0)$ are much higher than our corresponding values of ≈7.8 and ≈5.5, respectively. These differences in $\langle\varepsilon\rangle$ and the corresponding larger band gap (see previous discussion) are due to the film being a single crystal as opposed to the amorphous films used in this study. The energy position of the main $\langle\varepsilon_1\rangle$ peak position at about 6.6 eV observed for sample S19 (see Fig. 3) is similar to that of the single crystal of Lim *et al.*[23] as well as of sputtered HfO_2 (Ref. 27) and jet-vapor-deposited HfO_2.[9] Boher *et al.*[13] showed the k extinction coefficient peaked at ≈7.5 eV but decreased at a higher photon energy range (from 7.5 up to 9.0 eV). Our k (see the inset of Fig. 3) increases to a similar peak at 7.5 eV, but continues to increase above and beyond the experimental spectral range. It indicates there is another oscillator above 9.0 eV which is qualitatively consistent with the existence of a high interband transition from the oxygen $2p$ orbital to the Hf s orbital.[18] Further, a surface roughness layer determined from GXR data fitting was incorporated in the data analysis by Boher *et al.*,[13] indicating that the HfO_2 film surface deposited by sputtering appears to be rough compared with the films prepared by ALCVD employed in this study. On the other hand, Sun *et al.*[10] showed that the extinction coefficient k of their ALD HfO_2 also increases above the ≈7.5 eV peak in a good agreement with our HfO_2 results. This agreement implies that HfO_2 films grown by ALD are optically comparable, and their corresponding electronic structures are in agreement with the electronic orbital model of transitional metals.[18] It is desired that high-κ materials remain amorphous throughout the device fabrication process to avoid high-leakage current.[28] The dielectric functions, especially in the imaginary part $\langle\varepsilon_2\rangle$, have been reported to exhibit an additional and relatively sharp peak (≈5.9 eV) above the fundamental band gap when the films became polycrystalline under high-temperature annealing.[29] Our own most recent studies on jet-vapor-deposited polycrystalline Hf–aluminate films also displayed a shoulder peak at ~5.7 eV just above the band gap and below the main broader peak at ≈7.0 eV.[9] Based on the results of these previous reports on the polycrystalline HfO_2 films, our low temperature grown ALCVD films remain amorphous as evidenced by the absence of the 5.7 eV polycrystalline feature. The amorphous nature of these films is also clearly supported by the HRTEM images shown in Fig. 1. A similar conclusion was reached for ALD HfO_2/Al_2O_3 film stacks whereby cross-sectional HRTEM pictures of as-deposited HfO_2 on a nontreated reaction barrier Al_2O_3 layer had a completely amorphous structure.[30]

B. Optical band gap E_g and dielectric function of $(HfO_2)_x(Al_2O_3)_{1-x}$ alloy films

The effects of alloying with Al_2O_3 in the growth of $(HfO_2)_x(Al_2O_3)_{1-x}$ films on the optical band gap E_g and the pseudo dielectric functions are depicted in Figs. 5 and 6. A parabolic dependency of E_g on the Al density is clearly shown in Fig. 5, where the absolute areal densities Al were measured by NRA (see Table. I). On the other hand, in terms of relative Hf and Al composition, as seen in Fig. 6, the E_g varies *linearly* with the mole fraction x of HfO_2 in the $(HfO_2)_x(Al_2O_3)_{1-x}$ alloys, where x was calculated from the ratio of the Hf/Al areal densities measured by both RBS and NRA described previously. The fact that the band gap E_g increases with the higher Al_2O_3 mole fraction implies that a chemical intermixing of HfO_2 and Al_2O_3 occurred in the ALD processes. It is believed that the intermixing of these two transition metal oxides, with Al_2O_3 having a larger band gap, increases the separation of the oxygen $2p$ orbital valence band state and the antibonding d states intermixed of Hf and Al, and therefore results in a larger band gap.[18] Note that the endpoint (Al_2O_3 or $x=0, E_g=6.25$ eV) was not available in this study and was taken from our previous similar studies of HfAlO films grown by the jet-vapor deposition.[9] E_g of thin Al_2O_3 film has been observed to be smaller than that of bulk Al_2O_3 crystal,[26] indicating that the deposited oxides are structurally and electronically different from the bulk crystal of the same oxide. By using least squares fitting, we obtained $E_g=6.26-0.68x$ (eV) shown by the solid line in Fig. 6. In the study by Yu *et al.*[25] mentioned previously, XPS

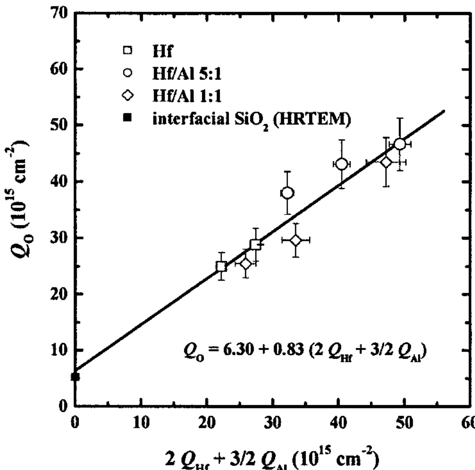

FIG. 7. Plot of Q_O versus $(2\ Q_{Hf}+2/3\ Q_{Al})$ where $Q_{O\ and\ Hf}$ are the elemental amounts (areal densities) calculated from the area of the channeling RBS signals and Q_{Al} profile determined by resonant NRA. Ideal $(HfO_2)_x(Al_2O_3)_{1-x}$ alloy films on Si yields a straight line of unit slope crossing the origin. A linear fit indicates a positive intercept at the y axis consistent with $\approx$12 Å of interfacial SiO_2.

data also show a linear relation, $E_g=6.52-1.27x$ (eV), depicted by the dashed line. Both studies agree in terms of the linear dependency of increasing band gap with increasing Al mole fraction. It is noted that, by extrapolating x to 0, we obtained the E_g value of 6.26 eV for the jet-vapor-deposited amorphous Al_2O_3 film, which is lower than that of 6.52 eV measured by XPS. However, the XPS data show that E_g started at a much lower value of 5.25 eV for the HfO_2 compared with the averaged $E_g(\sim5.56\ \text{eV})$ from samples S16 and S19 and increased at a higher rate. The origins of this discrepancy possibly stem from (i) the material quality and preparation methods used in each study, and (ii) the methodology of how E_g was deduced. The XPS-derived E_g relies on the onset of energy loss from energy-loss spectra of the core electron oxygen 1s energy-loss spectra, whereas E_g, deduced from the optical method, is commonly based on the optical energy absorption near the band gap. The latter method has been well established for amorphous materials (which were used in this study) which follow the Tauc-law formula described and used previously. Further, from Fig. 3, since overall the magnitude of $\langle\varepsilon_1\rangle$ and $\langle\varepsilon_2\rangle$ decreases and the Lorentz (second E_0 in the TL dispersion) oscillator peak position shifts to higher energy with increasing Al content, HfO_2 and Al_2O_3 are believed to be intermixed in the alloy.

Figure 7 presents the plot of oxygen atomic concentration (Q_O) versus $\left(2Q_{Hf}+\frac{2}{3}Q_{Al}\right)$. Ideal $(HfO_2)_x(Al_2O_3)_{1-x}$ alloy films on Si should yield a straight line of unit slope crossing the origin. A linear fit to our data indicates a positive intercept at the y axis consistent with an interfacial SiO_2 thickness of $\approx$12 Å, in very good agreement with HRTEM results (Fig. 1). The slope, 0.8, indicates that the films could be slightly oxygen deficient with respect to the prototypical ideal alloys. Al profiles are consistent with uniform distribution of Al in the films (within the resolution of NRA), with the exception of sample S24, in which an Al-containing layer is stacked between two Hf-containing layers.

At this juncture, it is important to point out the discrepancies that could arise from the inclusion of the SiO_2 interfacial layer in the SE model when comparing with the results otherwise obtained from the single-layer (without the interfacial layer) model. As described previously about the modeling of the SE data, the thickness of SiO_2 interface (from HRTEM) was used as a fixed value in the data analysis that determined the HfO_2 and Hf–aluminate layer thicknesses and their dielectric functions. However, with the single-layer model, we found that the resulting thicknesses for all samples were approximately 3% less than the sum of the thickness of the fixed SiO_2 interface and the film obtained from the two-layer model. In addition, the single-layer E_g's are approximately 0.05 eV larger than those deduced from the model with the fixed SiO_2 interfacial layer. However, the relative magnitudes in ε_1 and ε_2 and the value of E_g vary consistently with the relative amount of Al in the films in either model. It is also noticed that the film thicknesses of HfO_2 of sample S5 and HfAlO of sample S7 determined from the two-layer model are approximately 0.4 nm thicker than those obtained from the corresponding HRTEM. These differences could come from the different beam sizes employed in the SE and HRTEM. SE results are averaged over a much larger ($\approx$2 mm$\times$4 mm) area of the sample whereas HRTEM focuses on a much smaller area of $\approx$0.5 μm $\times 2\mu$m cross section. In addition, the boundary of the film at the interfaces may not be uniquely defined in the HRTEM images.

IV. SUMMARY

VUV-SE has been used to investigate the optical properties of a set of HfO_2 and Hf–aluminate films fabricated by ALCVD with various Al_2O_3 compositions. The modeling and data analyses were presented and shown to reproduce the experimental data very well. The various growth sequences, by changing the ratio of HfO_2 and Al_2O_3 precursors, produced different aluminum densities in the HfAlO films. RBS and resonant NRA measurements were performed to obtain the hafnium, oxygen, and aluminum concentrations and profiles. The determined complex pseudo dielectric functions $(\langle\varepsilon\rangle)$ by VUV-SE for all the HfO_2 and HfAlO films exhibit the shift of the fundamental band gap E_g from $\approx$5.56 eV of HfO_2 to $\approx$5.92 eV of HfAlO grown by a (1:1) ratio of HfO_2 and Al_2O_3 precursors. Also it was consistently observed that the magnitude of $\langle\varepsilon_1\rangle$ and $\langle\varepsilon_2\rangle$ decreased with increasing Al content in the films. In terms of the mole fraction of Al_2O_3 in the alloy $(HfO_2)_x(Al_2O_3)_{1-x}$, a linear relation, $E_g=6.26-0.68x$, was experimentally observed. However, E_g follows a parabolic function with respect to the areal density of aluminum. HRTEM images taken on the same samples revealed amorphous structure of as-grown ALCVD films, clearly confirming the amorphous characteristics observed in the dielectric functions determined by SE.

This study has demonstrated the powerful, nondestructive, and relatively economical capabilities of VUV-SE that can be used for *in situ* and online monitoring and/or controlling of the depositions of technically relevant high-*k* dielectric gates in advanced IC devices. Particularly, in addition to thickness measurements traditionally and routinely performed by ellipsometry in IC device fabrication, the band gap and the optical properties can be determined and then used as growth monitoring parameters to assess and control compositions as well as structural qualities of high-*k* films.

V. DISCLAIMER

Certain commercial equipment, instruments, or materials are identified in this paper in order to specify the experimental procedure adequately. Such identification is not intended to imply recommendation or endorsement by the National Institute of Standards and Technology, nor is it intended to imply that the materials or equipment identified are necessarily the best available for the purpose.

ACKNOWLEGMENTS

Three of the authors (N.V.N., J.R.E., and S.S.) express their appreciation and gratitude for the continuous financial support from the NIST Office of Microelectronics Programs (OMP). Another author (P.Y.H.) would like to thank Jeff Peterson for his discussion on the ALCVD process.

[1]R. M. Wallace and G. Wilk, MRS Bull. **27**, 212 (2002).
[2]*Semiconductor Industry Association, The International Technology Roadmap for Semiconductors*, 2001 Ed., (International SEMATECH, Austin, TX, 2001).
[3]C. A. Richter, A. R. Hefner, and E. M. Vogel, IEEE Electron Device Lett. **22**, 35 (2001).
[4]G. D. Wilk, R. M. Wallace, and J. M. Anthony, J. Appl. Phys. **89**, 5243 (2001).
[5]D. G. Schlom and J. H. Haeni, MRS Bull. **27**, 198 (2002).
[6]W. J. Zhu, T. Tamagawa, M. Gibson, T. Furukawa, and T. P. Ma, IEEE Electron Device Lett. **23**, 649 (2002).
[7]M.-Y. Ho, H. Gong, G. D. Wilk, W. W. Busch, M. L. Green, W. H. Lin, A. See, S. K. Lahiri, M. E. Loomans, Petri I. Räisänen, and T. Gustafsson, Appl. Phys. Lett. **81**, 4218 (2002).
[8]H. Y. Yu, N. Wu, M. F. Li, C. Zhu, B. J. Cho, D.-L Kwong, C. H. Tung, J. S. Pan, J. W. Chi, W. D. wang, D. Z. Chi, C. H. Ang, J. Z. Zeng, and S. Ramantan, Appl. Phys. Lett. **81**, 3618 (2002).
[9]N. V. Nguyen, J.-P. Han, J. Y. Kim, E. Wilcox, Y. J. Cho, W. Zhu, Z. Luo, and T. P. Ma, *Characterization and Metrology for ULSI Technology*, International Conference, edited by D. G. Seiler, A. C. Diebold, T. J. Shaffner, R. McDonald, S. Zollner, R. P. Khosla, and E. M. Secula (AIP Press, Melville, NY, 2003), pp. 181–185.
[10]L. Sun, C. Defranoux. J. L. Stehle, P. Boher, P. Evrard, E. Bellandi, and H. Bender, Mater. Res. Soc. Symp. Proc. **786**, E3.29.1 (2004).
[11]S.-G. Lim, S. Kriventsov, T. N. Jackson, J. H. Haeni, G. G. Schlom, A. M. Balbashov, R. Uecker, P. Reiche, J. L. Freeouf, and G. Lucovsky, J. Appl. Phys. **91**, 4500 (2002).
[12]J. N. Hilfiker, C. L. Bungay, R. A. Synowicki, T. E. Tiwald, C. M. Herzinger, B. Johs, G. K. Pribil, and J. A. Woollam, J. Vac. Sci. Technol. A **21**, 1103 (2003).
[13]P. Boher, P. Evrard, J. P. Piel, C. Defranoux, J. C. Fouere, E. Bellandi, and H. Bender, *Characterization and Metrology for ULSI Technology*, International Conference, edited by D. G. Seiler, A. C. Dielbold, T. J. Shaffner, R. McDonald, S. Zollner, R. P. Khosla, and E. M. Secula (AIP Press, Melville, NY, 2003), pp. 148–153.
[14]W. F. A. Besling, E. Young, T. Conard, C. Zhao, R. Carter, W. Vandervorst, M. Caymax, S. De. Gendt, M. Heyns, J. Maes, M. Tuominen, and S. Haukka, J. Non-Cryst. Solids **303**, 123 (2002).
[15]M. Copel, M. Gribelyuk, and E. Gusev, Appl. Phys. Lett. **76**, 436 (2000).
[16]B. Johs, J. A. Woollam, C. M. Herzinger, J. Hilfiker, R. Synowicki, and C. L. Bundgay, Proc. SPIE **CR72**, 29 (1999).
[17]G. E. Jellison, Jr. and F. A. Modine, Appl. Phys. Lett. **69**, 371 (1996); **69**, 2137 (1996).
[18]G. Lukovsky, J. L. Whitten, and Y. Zhang, Microelectron. Eng. **59**, 329 (2001).
[19]G. Lucovsky, J. L. Whitten, and Y. Zhang, Solid-State Electron. **46**, 1687 (2002).
[20]A. S. Ferlauto, G. M. Ferreira, J. M. Pearce, C. R. Wrongski, R. W. Collins, X. Deng, and G. Ganguly, J. Appl. Phys. **92**, 2424 (2002).
[21]J. Tauc, R. Grigorovici, and A. Vancu, Phys. Status Solidi **15**, 627 (1966).
[22]M. Balog, M. Schieber, M. Michman, and S. Patai, Thin Solid Films **41**, 247 (1977).
[23]S.-G. Lim, S. Kriventsov, T. N. Jackson, J. H. Haeni, D. G. Schlom, A. M. Balbashov, J. L. Freeouf, and G. Lucovsky, J. Appl. Phys. **91**, 4500 (2002).
[24]M. Modreanu, P. K. Hurley, B. J. O'Sullivan, B. O'Looney, J. P. Senateur, H. Rousell, F. Rousell, M. Audier, C. Dubourdieu, I. W. Boyd, Q. Fang, T. L. Leedham, S. Rushworth, A. C. Jones, H. Davies, and C. Jimenez, Proc. SPIE **4876**, 1236 (2002).
[25]H. Y. Yu, F. Li, B. J. Cho, C. C. Yeo, M. S. Joo, D.-L. Kwong, J. S. Pan, C. H. Ang, J. Z. Zheng, and S. Ramanathan, Appl. Phys. Lett. **81**, 376 (2002).
[26]V. V. Afanas'ev and A. Stesmans, Appl. Phys. Lett. **82**, 245 (2003).
[27]P. Boher, P. Evrard, J. P. Piel, J. L. Stehle, J. Non-Cryst. Solids **303**, 167 (2002).
[28]W. J. Zhu, T. Tamagawa, G. Gibson, T. Furukawa, and T. P. Ma, IEEE Electron Device Lett. **23**, 649 (2002).
[29]Y. J. Cho, N. V. Nguyen, C. A. Richter, J. R. Ehrstein, B. H. Lee, and J. C. Lee, Appl. Phys. Lett. **80**, 1249 (2001).
[30]H. B. Park, M. Cho, J. Park, S. W. Lee, C. S. Hwang, and J. Jeong, Electrochem. Solid-State Lett. **7**, F25 (2004).